Applied Surface Science 268 (2013) 87–91

Contents lists available at SciVerse ScienceDirect

Applied Surface Science

journal homepage: www.elsevier.com/locate/apsusc

Stability and electronic properties of polar and non-polar surfaces of CuI

Jiajie Zhu [a], Mu Gu [a,*], Ravindra Pandey [b,*]

[a] Department of Physics, Tongji University, Shanghai 200092, PR China
[b] Department of Physics, Michigan Technological University, Houghton 49931, MI, USA

ARTICLE INFO

Article history:
Received 19 September 2012
Received in revised form
29 November 2012
Accepted 30 November 2012
Available online 20 December 2012

Keywords:
CuI
Surfaces
Stability
Electronic properties

ABSTRACT

The structural and electronic properties of polar and non-polar surfaces of CuI are investigated at the GGA-DFT level of theory. The results find that the stability of the surfaces is directly related to the interplanar distance as well as the atomic character of the terminating layer. The I-terminated surfaces are predicted to be energetically preferred. We predict the instability of the Cu-terminated (1 1 1) surface, whereas the nonpolar (1 1 0) surface shows a significant surface reconstruction with a large layer rotation angle. The Cu-terminated and I-terminated ($\bar{1}\,\bar{1}\,\bar{1}$) surfaces prefer to retain their bulk-like configurations, whereas the Cu-terminated (0 0 1) and (0 0 $\bar{1}$) surfaces show large deviations from their bulk configurations. The calculated band gap shows a blue or red shift of the absorption edge relative to the bulk CuI depending on the atomic nature of the terminating surface.

1. Introduction

Cuprous iodine (CuI) is a well-known p-type semiconductor with a large gap of 3.1 eV [1]. The bulk CuI also facilitates the study of the exciton–exciton scattering processes in semiconducting materials due to its large exciton binding energy of 62 meV [2]. Recently, the scintillation properties of CuI have drawn much attention due to its ultrafast decay time of 420–430 nm emission [3,4]. Note that scintillators used for detection of the high-energy rays such as X-rays, gamma-rays etc. are required to have fast decay time to realize high time resolution.

Since thin films of CuI are proposed as a candidate material for applications in optoelectronic devices such as dye-sensitized solar cell [5], their fabrication and characterization have been performed by several research groups [6–9]. For example, Sirimanne et al. prepared the normal (1 1 1) oriented film using the pulse laser deposition technique [6]. Zheng et al. fabricated the (1 1 0) oriented film and found that the intensity of the emission at 420 nm is closely related to the orientations of the films [9]. It was suggested that the growth orientation of CuI film is closely related to the stability of the surfaces [10]. Note that the theoretical model [10] employed was somewhat limited in considering the interaction of the adsorbed atoms and the surface layer of the as grown crystal ignoring the contributions from the inner layers. Electronic structures of CuI films were probed yielding the values of the band gap ranging from 2.9 eV to 3.5 eV which are different from the bulk value of 3.1 eV [7]. This may be due to the fact that the orientations of the fabricated thin films can influence the electronic properties.

Considering that the electronic structures such as the band gap and the effective mass of hole directly determine the exciton energy and the conductivity of CuI films, we embark upon a detailed investigation of the polar and nonpolar surfaces of the zinc-blende CuI. We note that there exists a lack of theoretical studies predicting the stability and electronic properties of the polar and non-polar surfaces of CuI. Furthermore, a complete understanding of surface properties including surface reconstruction and band structure is a prerequisite for the development of CuI-based devices.

We use first-principles method to calculate the atomic structures and electronic properties of zinc-blende CuI surfaces including Cu-terminated and I-terminated (0 0 1), Cu-terminated and I-terminated (0 0 $\bar{1}$), nonpolar (1 1 0), Cu-terminated and I-terminated (1 1 1) and Cu-terminated and I-terminated ($\bar{1}\,\bar{1}\,\bar{1}$) surfaces. It is to be noted here that CuI crystallizes in the zinc-blende structure at ambient condition, though it can be transformed into several polymorphs at high-temperature and high-pressure. Our group has recently performed a comprehensive theoretical study of polymorphs of CuI providing a very good description of their structural, elastic, electronic and optical properties [11].

2. Computational method

We use the projector augmented plane-wave (PAW) method as implemented in Vienna *ab initio* simulation package (VASP) [12,13] to investigate the stability and electronic properties of the CuI

* Corresponding authors.
E-mail addresses: mgu@tongji.edu.cn (M. Gu), pandey@mtu.edu (R. Pandey).

0169-4332/$ – see front matter © 2012 Elsevier B.V. All rights reserved.
http://dx.doi.org/10.1016/j.apsusc.2012.11.171

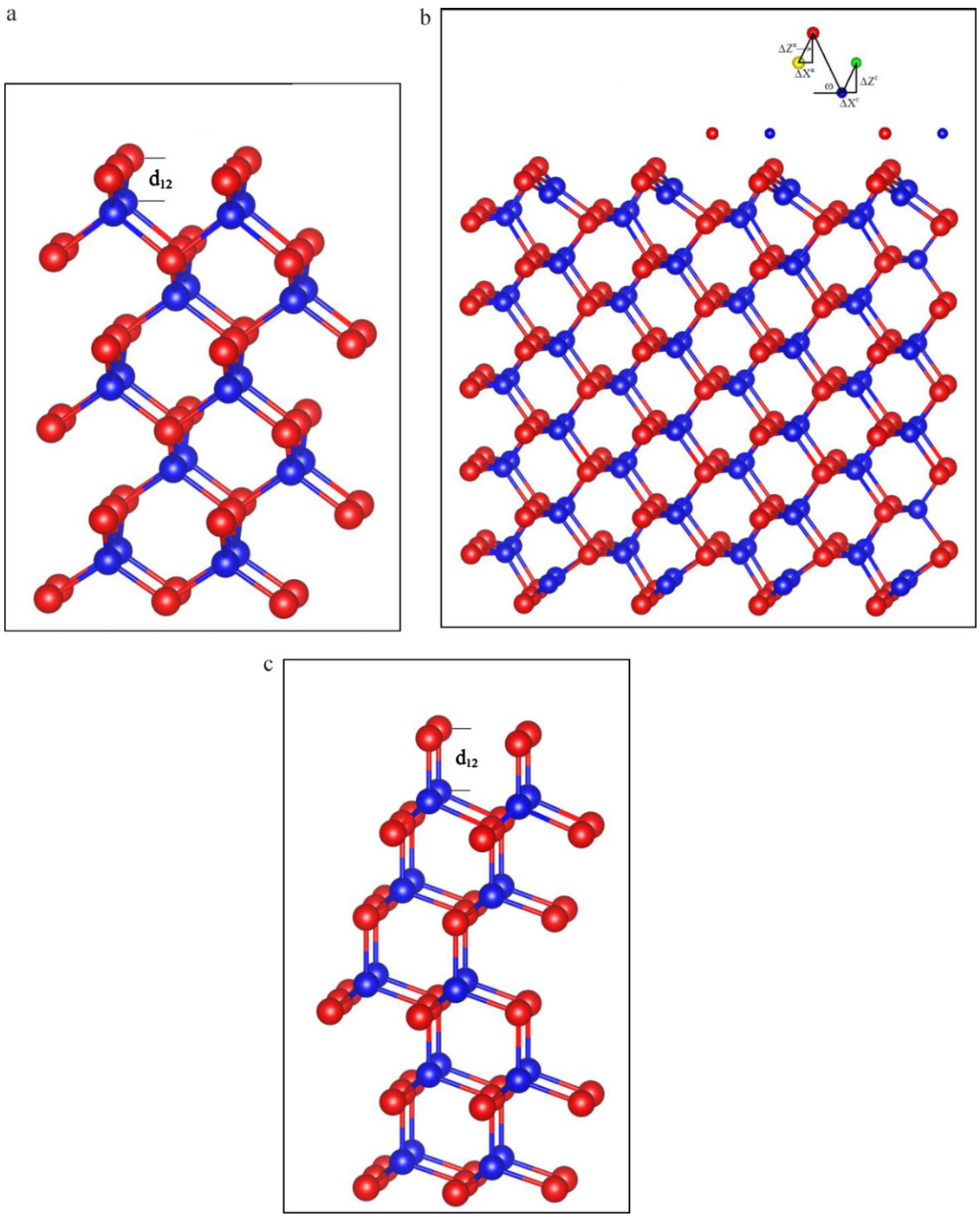

Fig. 1. A schematic diagram of (a) I-terminated (0 0 1), (b) (1 1 0) and (c) I-terminated (1 1 1) surfaces. The interplanar distances between the first and the second layers of I-terminated (0 0 1) and (1 1 1) surfaces are labeled as d_{12}. The reconstruction of (1 1 0) surface (first and second layers) is illustrated in the inset of (b). The horizontal and vertical relaxations of surface cations and anions from their equilibrium positions defined as (ΔXc, ΔZc) and (ΔXa. ΔZa), respectively.

surfaces. The generalized gradient approximation (GGA) of Perdew, Burke and Ernzerhof (PBE) is adopted for the exchange-correlation potential to the density functional theory (DFT) [14]. We treat the 3d and 4s electrons of Cu together with 5s and 5p electrons of I as the valance electrons in the electronic structure calculations.

In order to validate the accuracy and reliability of the modeling elements, we have performed the calculations of the bulk CuI at the GGA (PBE)-DFT level of theory. The calculated structural properties for the zinc-blende CuI are in excellent agreement with the experimental values. For example, the lattice constant is calculated to be 6.074 Å. The corresponding experimental value is 6.054 Å. Likewise, the calculated and experimental values of the bulk modulus are 39.1 and 36.6 GPa, respectively [11,15].

We use 2-dimensional periodic slab model consisting of eleven layers separated by a vacuum region of 23 Å to simulate the stoichiometric (1 1 0) surface and nonstoichiometric Cu-terminated and I-terminated (0 0 1), (0 0 $\bar{1}$), (1 1 1) and ($\bar{1}$ $\bar{1}$ $\bar{1}$) surfaces of CuI. Such a large number of layers ensure the convergence of the surface energy with respect to the slab thickness. Note that the slabs are symmetric for (1 1 0) surface, but asymmetric for (0 0 1) and (1 1 1) surfaces. Each layer in the slab of the (0 0 1), (0 0 $\bar{1}$), (1 1 1) and ($\bar{1}$ $\bar{1}$ $\bar{1}$) surfaces has only one kind of atom whereas

the (1 1 0) surface is nonpolar consisting of both Cu and I atoms (Fig. 1).

The surface geometry optimization calculation begins with the ideal surface having atomic geometry of the bulk CuI. The surface atoms associated with first, second and third layers are then allowed to relax until the force on each atom is less than 0.01 eV/Å. It is estimated to lead to the numerical uncertainty of about 0.01 Å in atomic displacement. The Brillouin-zone integrations are carried out with $8 \times 8 \times 1$ k-point mesh. The cut-off energy for plane-wave basis is 355 eV. The energy tolerance is 10^{-6} eV in the iterative solution of Kohn-Sham equations.

We define the surface free energy as [16]

$$F = \frac{1}{2A}(E_{\text{slab}} - \sum_i n_i \mu_i), \quad (1)$$

where E_{slab} is the total energy of the slab, A is the surface area of the slab and n_i and μ_i are the number and chemical potential of atom i.

The chemical potentials of Cu and I atoms are limited by following conditions.

$$\mu_{\text{Cu}} + \mu_{\text{I}} = E(\text{CuI}) \quad (2)$$

$$\mu_{\text{Cu}} \leq E(\text{Cu}) \quad (3)$$

$$\mu_{\text{I}} \leq E(\text{I}) \quad (4)$$

where E(Cu), E(I) and E(CuI) are the total energies of bulk Cu, I and CuI, respectively.

The chemical potentials are given by

$$\mu_{\text{Cu}} = E(\text{Cu}) \quad (5)$$

$$\mu_{\text{I}} = E(\text{CuI}) - E(\text{Cu}) \quad (6)$$

under the Cu-rich limit and

$$\mu_{\text{I}} = E(\text{I}) \quad (7)$$

$$\mu_{\text{Cu}} = E(\text{CuI}) - E(\text{I}) \quad (8)$$

under the I-rich limit.

For the nonpolar (1 1 0) surface, the horizontal and vertical relaxations of cations and anions from their equilibrium positions are defined as (ΔX^c, ΔZ^c) and (ΔX^a. ΔZ^a), respectively (Fig. 2). Note that the horizontal relaxation of the (1 1 0) surface is along the [0 0 1] direction. The layer rotation angle and change in the near-neighbor distance are given by ω (Fig. 2) and $\Delta R_{\text{surface}}$, respectively [17]. For other surfaces, the relaxation is defined by the shifts of the first (Δd_1) and second layer (Δd_2). The positive and negative values of Δd_1 and Δd_2 represent the outward and inward shift, respectively. d_{12} refers to the interplanar distance between the first and second layers and Δd_{12} refers to its variation with respect to the bulk value.

3. Results and discussion

3.1. Structural properties

Table 1 displays the calculated structural parameters for the (1 1 0) surface of CuI. The horizontal and vertical displacements of Cu atom on the first layer are predicted to be much larger than that associated with I atom. The relaxations of the atoms on second layer are small. The surface buckling which is the sum of the vertical distance of the anion and cation on the top surface layer is calculated to be 0.85 Å (Table 1).

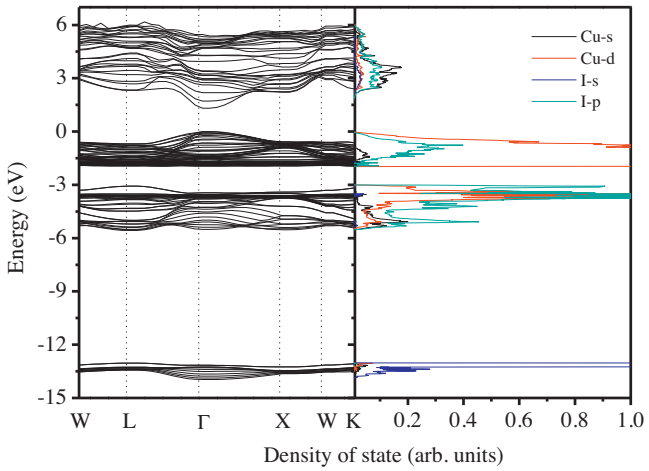

Fig. 2. The calculated band structure and atomic projected density of state of (1 1 0) surface of CuI. Zero of the energy is aligned to the valance band maximum (VBM).

Table 2
Calculated structural properties of the relaxed (0 0 1), (1 1 1), and ($\bar{1}\,\bar{1}\,\bar{1}$) surfaces of CuI. Δd_1 and Δd_2 are shifts of the first and second layers, respectively. A positive value represents an outward shift and a negative value represents an inward shift of surface atoms. d_{12} and Δd_{12} refer to the interplanar distance and its variation from the bulk configuration of CuI.

	Δd_1 (Å)	Δd_2 (Å)	d_{12} (Å)	Δd_{12} (Å)
Cu-terminated (0 0 1)	−0.61	−0.34	1.25	−0.27
Cu-terminated (0 0 $\bar{1}$)	−0.12	0.15	1.25	−0.27
I-terminated (0 0 1)	0.27	0.38	1.41	−0.11
I-terminated (0 0 $\bar{1}$)	−0.07	0.03	1.42	−0.10
Cu-terminated ($\bar{1}\,\bar{1}\,\bar{1}$)	−0.03	0.02	2.58	0.05
I-terminated ($\bar{1}\,\bar{1}\,\bar{1}$)	0.05	0.09	0.84	0.04
I-terminated (1 1 1)	0.04	0.21	2.46	0.17

The calculated value of the layer rotation angle, ω is 37.8°. It is much larger than the previously reported value of 4.8° obtained using the pseudo-function method within the framework of the local density approximation (LDA) to density functional theory [18]. Note that the LDA-DFT values of ω for CuCl and CuBr are −0.13° and 1.5°, respectively, which are significantly different from the values of 53° and 35° obtained from the low-energy electron diffraction (LEED) experiments [19]. Thus, our calculated ω appears to be reasonable, though no experimental measurement is available for the (1 1 0) surface of CuI. Furthermore, the bond contraction of the first layer is calculated to be 3.3%. It is smaller than that of CuCl (≈8.6%) due to the low value of the Phillip's iconicity for CuI [20].

Table 2 lists the calculated structural properties of the (0 0 1), (0 0 $\bar{1}$), (1 1 1) and ($\bar{1}\,\bar{1}\,\bar{1}$) surfaces of CuI. For the Cu-terminated (0 0 1) and (0 0 $\bar{1}$) surfaces, d_{12} decreases by 0.61 Å. This is not the case with the Cu-terminated ($\bar{1}\,\bar{1}\,\bar{1}$) surface where the interplanar distance prefers the bulk-like configuration. This contrasting behavior is partly due to geometrical differences between the (0 0 1) and (0 0 $\bar{1}$) surfaces. For example, d_{12} values of the ideal (0 0 1) and (0 0 $\bar{1}$) surfaces are only 58% of the bulk Cu–I separation, whereas

Table 1
Calculated structural properties of the relaxed CuI (1 1 0) surface: (ΔX^c, ΔZ^c), (ΔX^a and ΔZ^a) are the horizontal and vertical displacements of cations and anions, respectively from their equilibrium positions. ω and $\Delta R_{\text{surface}}$ are the layer rotation angle and change in the near-neighbor distance at the surface, respectively.

	ΔX^c (Å)	ΔZ^c (Å)	ΔX^a (Å)	ΔZ^a (Å)	ω (deg)	$\Delta R_{\text{surface}}$ (%)
Surface layer (top layer)	−0.48	−0.71	−0.06	0.13	37.8	3.3
Bulk-like layer (layer 2)	0.11	0.05	0.05	−0.07	–	–

Table 3
Calculated free energy of CuI – (0 0 1), (1 1 0) and (1 1 1) surfaces.

	Surface free energy (meV/Å^2)	
	Cu rich	I rich
(1 1 0)	4.8	4.8
Cu-terminated (0 0 1)	94.7	103.3
I-terminated (0 0 1)	4.2	−5.0
Cu-terminated (1 1 1)	100.4	111.0
I-terminated (1 1 1)	10.8	0.36

d_{12} of the Cu-terminated $(\bar{1}\,\bar{1}\,\bar{1})$ surface is similar to the bulk Cu–I bond-distance. Thus, a significantly larger Coulomb attraction acts between Cu^+ and I^- ions for the (0 0 1) and $(0\,0\,\bar{1})$ surfaces. We note that geometrical relaxation of the Cu-terminated (1 1 1) surface leads to collapsing of the second layer to the surface layer due to much smaller interplanar spacing ($d_{12} \approx 33\%$ of the bulk Cu—I bond distance).

For the I-terminated (0 0 1) and $(0\,0\,\bar{1})$ surfaces, d_{12} contracts less than that in the Cu-terminated (0 0 1) and $(0\,0\,\bar{1})$ surfaces. On the other hand, the I-terminated $(\bar{1}\,\bar{1}\,\bar{1})$ surface yields a similar Δd_{12} as predicted for the Cu-terminated $(\bar{1}\,\bar{1}\,\bar{1})$ surface. Although the Columbic attraction from second layer is much weaker in the case of the I-terminated (1 1 1) surface, d_{12} still retains the bulk-like configuration. Note that one cannot define surface buckling for the (0 0 1), $(0\,0\,\bar{1})$, (1 1 1), and $(\bar{1}\,\bar{1}\,\bar{1})$ surfaces, because each layer is consisted of only single atom.

Bader's charge analysis is performed to examine the charge transfer between the terminating surface layer and the inner layers of the asymmetric slabs. For the I-terminated surfaces, the charge transfer from the inner bulk-like layers to the terminating surface layer is about 0.08 e. No charge transfer takes place for the Cu-terminated (0 0 1) surface.

The calculated values of the surface free energy are listed in Table 3. For non-stoichiometric cases, we give values for both Cu-rich and I-rich limits, as their free energies are related to the atomic chemical potentials (Eqs. (5)–(8)). Overall, the I-terminated (0 0 1) surface is predicted to be the most stable surface for CuI.

In a previous theoretical study [11], the stability of the Cu-terminated (1 1 1) surface was predicted to be same as that of the I-terminated $(\bar{1}\,\bar{1}\,\bar{1})$ surface. It was argued that the stability of the given surface atom mainly depends on the coordination number of the surface atom. The surface atoms of the Cu-terminated (1 1 1) and the I-terminated $(\bar{1}\,\bar{1}\,\bar{1})$ surfaces have the same coordinate number.

In general, stability of the surface (i.e. first layer) depends not only on the near-neighbor atoms but also on the next-nearest atoms. Thus, the interaction between the first and second layers of both Cu-terminated and I-terminated surfaces is governed by the Cu–I interaction. However, the second-neighbor interactions for both surfaces are different as they involve either Cu–Cu or I–I interaction yielding a difference in the stability of the Cu-terminated (1 1 1) and I-terminated $(\bar{1}\,\bar{1}\,\bar{1})$ surfaces. The calculated results therefore find that stability of the surface is directly related to the interplanar distance between the first and second layers as well as the atomic character of the terminating surface layer.

3.2. Electronic properties

The calculated density of states (DOS) and band structures of CuI surfaces are shown in Figs. 2–5. We note that the uppermost valence band is mainly formed by Cu-3d with a smaller contribution from I-5p states. However, the character of the valence band maximum (VBM) of the (0 0 1) and (1 1 1) surfaces depends on the terminating surface layer; it is Cu-3d states for the Cu-terminated surface and the hybridized Cu-3d and I-5p states for

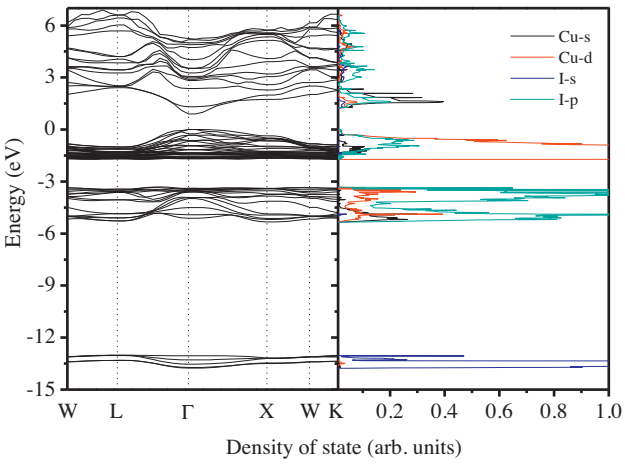

Fig. 3. The calculated band structure and atomic projected density of state of Cu-terminated (0 0 1) surface of CuI. Zero of the energy is aligned to the valance band maximum (VBM).

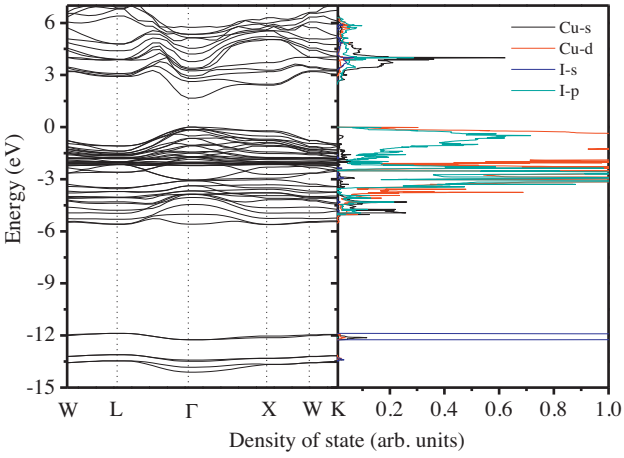

Fig. 4. The calculated band structure and atomic projected density of state of I-terminated (0 0 1) surface of CuI. Zero of the energy is aligned to the valance band maximum (VBM).

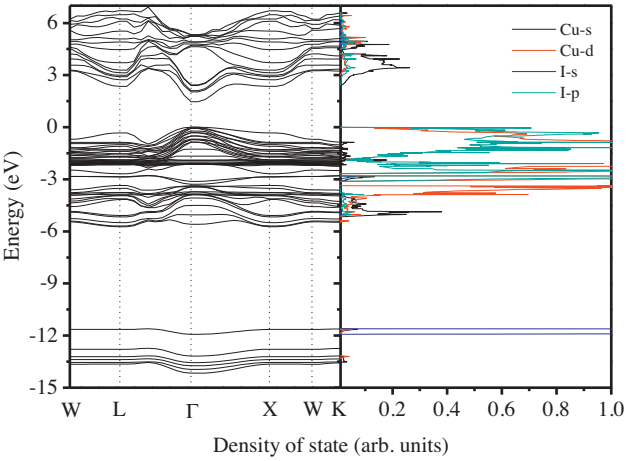

Fig. 5. The calculated band structure and atomic projected density of state of I-terminated (1 1 1) surface of CuI. Zero of the energy is aligned to the valance band maximum (VBM).

Table 4
Calculated band gaps and effective mass of electrons and holes of the relaxed (0 0 1), (1 1 1) and (1 1 0) surfaces of CuI at the GGA-DFT level of theory.

	Cu-terminated (0 0 1)		I-terminated (0 0 1)		I-terminated (1 1 1)		(1 1 0)		Bulk CuI [6]	
Band gap (eV)	0.9		1.67		1.46		1.32		1.13	
Effective mass (m_e)	Γ-L	Γ-X	Γ-L	Γ-X	Γ-L	Γ-X	Γ-L	Γ-X	Γ-L	Γ-X
Electron	0.44	0.42	0.58	0.58	0.47	0.43	0.41	0.44	0.34	0.33
Light hole	0.63	0.45	1.06	0.65	0.98	0.84	0.88	1.63	0.38	0.50
Heavy hole	1.59	9.40	1.40	9.09	5.67	7.03			3.14	1.54

the I-terminated surfaces of CuI. On the other hand, the character of the conduction band minimum (CBM) remains the same for the surfaces considered being composed of the Cu-4s states. Furthermore, a comparison of the surface band structures with the bulk band structure reveals a red shift in the absorption edge for the Cu-terminated (0 0 1) surface whereas the other surfaces show a blue shift in the absorption edge. A shift of the lower valence band consisting of the I-5s sates is also predicted. It is 1.3 and 1.6 eV for the I-terminated (0 0 1) and (1 1 1) surfaces, respectively.

Note that the band structures of the (1 1 0) and Cu-terminated (0 0 1) surfaces are found to be quite different from that of the other surfaces (Figs. 2 and 3). For example, the I-5p and Cu-3d bands appear in the lower valence band region (−2 eV to −3 eV from VBM) for the I-terminated (0 0 1) and (1 1 1) surfaces. These bands are associated with the surface atoms, as indicated in Figs. 4 and 5. However, no such band appears in the lower valence band of the (1 1 0) surface of CuI due to absence of the unsaturated (dangling) surface bond.

The calculations find the surfaces of CuI to be a direct gap with gaps ranging from 0.9 to 1.67 eV. It is similar to the values reported previously [21], though the experimental value is 3.1 eV. It should be pointed out that the GGA-DFT method underestimates the band gaps of the semiconducting and ionic materials. Nevertheless distinct features in the band structures of the CuI surfaces are clearly demonstrated by the method employed here.

The effective mass of electron and hole of different surfaces are also listed in Table 4. The effective mass is calculated by fitting the band structure in the vicinity of VBM and CBM using a parabolic function. For the CuI surfaces considered, the effective mass of electron appears to be more isotropic than that of the hole. The effective mass of both electron and hole on different surfaces is larger than that in the bulk, predicting a slower mobility of carriers on the surfaces of CuI relative to that in the bulk CuI.

4. Summary

The structural and electronic properties of (0 0 1), (0 0 $\bar{1}$), (1 1 0), (1 1 1) and ($\bar{1}$ $\bar{1}$ $\bar{1}$) surfaces of CuI are investigated in the framework of the GGA-DFT level of theory. I-terminated surfaces of CuI are predicted to be energetically preferred. The interplanar distance between the first and second layers of Cu-terminated and I-terminated ($\bar{1}$ $\bar{1}$ $\bar{1}$) surfaces retains the bulk configuration, but the Cu-terminated (0 0 1) and (0 0 $\bar{1}$) surfaces show a larger contraction from the bulk-like configuration. A significantly large layer rotation angle is also predicted for the nonpolar (1 1 0) surface. Since the Cu-terminated (1 1 1) surface is predicted to be not stable, the results suggest the growth along ($\bar{1}$ $\bar{1}$ $\bar{1}$) direction instead of [1 1 1] direction for thin films of CuI.

A blue shift of the exciton energy is predicted for thin films of CuI since the calculated band gap of the (1 1 0) surface is larger than that of the bulk CuI. A large band gap together with a large hole effective mass suggests a higher resistivity of thin films relative to that of the bulk in corroboration with the experimental results [8,22].

Acknowledgments

This work is funded by the National Natural Science Foundation of China (grant no. 91022002, 11179019), Significant National Special Project of the Ministry of Science and Technology of China for Development of Scientific Instruments and Equipment (grant no. 2011YQ13001902) and the Innovation Program of Shanghai Municipal Education Commission (grant no. 11ZZ29). Jiajie Zhu acknowledges the hospitality of Michigan Technological University.

References

[1] S. Lewonczuk, J. Ringeissen, E. Beaurepaire, M.A. Khan, Physical Review B 49 (1994) 2344–2350.
[2] H. Ichida, Y. Kanematsu, T. Shimomura, K. Mizoguchi, D. Kim, M. Nakayama, Physical Review B 72 (2005) 045210.
[3] P. Gao, M. Gu, X. Liu, B. Liu, S. Huang, Applied Physics Letters 95 (2009) 221904.
[4] S.E. Derenzoa, M.J. Weber, M.K. Klintenberg, Nuclear Instruments and Methods in Physics Research: Section A 486 (2002) 214–219.
[5] V.P.S. Perera, K. Tennakone, Solar Energy Materials and Solar Cells 79 (2003) 249–255.
[6] P.M. Sirimanne, M. Rusop, T. Shirata, T. Soga, T. Jimbo, Chemical Physics Letters 366 (2002) 485–489.
[7] N.A. Muhamad, M.A. Azman, U.M. Noor, M.R. Mahmood, Advanced Materials Research 403–408 (2012) 451–455.
[8] T. Tanaka, M. Hirose, K. Kawabata, Thin Solid Films 281 (1996) 179–181.
[9] Z. Zheng, A. Liu, S. Wang, B. Huang, K.W. Wong, X. Zhang, S.K. Hark, W.M. Lau, Journal of Materials Chemistry 18 (2008) 852–854.
[10] W.J. Li, E.W. Shi, Crystal Research and Technology 37 (2002) 1041–1048.
[11] J. Zhu, M. Gu, R. Pandey, Journal of Physics: Condensed Matter 24 (2012) 475503.
[12] G. Kresse, J. Furthmuller, Physical Review B 54 (1996) 11169–11186.
[13] G. Kresse, D. Joubert, Physical Review B 59 (1999) 1758–1775.
[14] J.P. Perdew, K. Burk, M. Ernzerhof, Physical Review Letters 77 (1996) 3865–3868.
[15] S. Hull, D.A. Keen, Physical Review B 50 (1994) 5868–5885.
[16] N. Moll, A. Kley, E. Pehlke, M. Scheffler, Physical Review B 54 (1996) 8844–8855.
[17] R. Pandey, P. Zapol, M. Causa, Physical Review B 55 (1997) R16009–R16012.
[18] M.H. Tsai, J.D. Dow, R.P. Wang, R.V. Kasowski, Physical Review B 40 (1989) 9818–9823.
[19] C.B. Duke, A. Paton, A. Lazarides, A. Kahn, Physical Review B 54 (1996) 14692–14702.
[20] D.L. Lessor, C.B. Duke, A. Kahn, W.K. Ford, Journal of Vacuum Science and Technology A 11 (1993) 2205–2209.
[21] B. Amrani, T. Benmessabih, M. Tahiri, I. Chiboub, S. Hiadsi, F. Hamdache, Physica B 381 (2006) 179–186.
[22] D. Chen, Y. Wang, Z. Lin, J. Huang, X. Chen, D. Pan, F. Huang, Crystal Growth and Design 10 (2010) 2057–2060.